Near-infrared frequency comb generation in mid-infrared interband cascade lasers

Lukasz A. Sterczewski,[1] Mahmood Bagheri,[1,*] Clifford Frez,[1] Chadwick L. Canedy,[2] Igor Vurgaftman,[2] Mijin Kim,[3] Chul Soo Kim,[2] Charles D. Merritt,[2] William W. Bewley,[2] and Jerry R. Meyer[2]

[1]*Jet Propulsion Laboratory, California Institute of Technology, Pasadena, CA 91109, USA*
[2]*Naval Research Laboratory, Washington, DC 20375, USA*
[3]*KeyW Corporation, Hanover, MD 21076, USA*
**Corresponding author: Mahmood.bagheri@jpl.nasa.gov*

Received 6 August 2019; revised 8 October 2019; accepted 11 October 2019; posted 31 October 2019; published 27 November 2019

The interband cascade laser (ICL) is an ideal candidate for low-power mid-infrared frequency comb spectroscopy. In this work, we demonstrate that its intracavity second order optical nonlinearity induces a coherent up-conversion of the generated mid-infrared light to the near-infrared through second-harmonic and sum-frequency generation. 10 milliwatts of light at 3.6 μm convert into sub-nanowatt levels of optical power at 1.8 μm, spread across 30 nm of spectral coverage. The observed linear-to-nonlinear conversion efficiency exceeds 3 μW/W^2 in continuous wave operation. We use a dual-band ICL frequency comb source to characterize water vapor absorption in both spectral bands.

This is a preprint version of the paper. For the final published version, please go to: http://dx.doi.org/10.1364/OL.44.005828

Since a seminal paper by Franken et al. [1] reported in 1961 the demonstration of second harmonic generation in a quartz crystal illuminated by a ruby laser that was invented just a year earlier [2], nonlinear optics (NLO) has formed a core of contemporary laser technology. Nonlinear frequency conversion has opened new avenues in ultrafast science by enabling studies in the attosecond regime [3], and has triggered substantial advances in disciplines ranging from biology to electronics [4]. NLO remains relevant because lasing at certain wavelengths is difficult or simply impractical, whereas nonlinear conversion from a more mature spectral region can be much more convenient.

Second order optical nonlinearities ($\chi^{(2)}$) in crystals such as lithium niobate ($LiNbO_3$) and potassium titanyl phosphate (KTP) have been widely exploited in modern optics for frequency doubling, parametric down conversion and sum-/ difference-frequency generation. Recently, nonlinear optical devices have been miniaturized on a host of chip-scale platforms, and reductions in the optical power thresholds for nonlinearities have followed [5]. However, most such sources rely on two separate components for the optical pump and nonlinear optical element, adding a layer of complexity to the on-chip integration. In this context, monolithic electrically-pumped semiconductor lasers with intrinsically large intracavity nonlinearities are of particular interest, since they merge both functions in a single device. Because the nonlinearities encountered in quantum well structures are typically orders of magnitude higher than those in conventional bulk optical crystals, the nonlinear interactions in semiconductor lasers can occur over short interaction lengths and under continuous wave operation [6]. Another advantage is the tailorability of nonlinearities through quantum engineering. In a pioneering experiment from 2003, Owschimikow et al. demonstrated intracavity sum-frequency generation (SFG) and second-harmonic generation (SHG) in a mid-infrared dual-wavelength multimode quantum cascade laser (QCL) [7]. This was soon followed by difference frequency generation (DFG) for THz generation [8,9] and theoretical studies of third-harmonic generation (THG) to reach the near-infrared region [10]. Optimization of the QCL design and careful intracavity phase-matching led eventually to significant improvements in the efficiencies of multi-band laser sources [11]. Very recently, intracavity DFG based on a second-order nonlinearity $\chi^{(2)}$ produced a room-temperature terahertz QCL frequency comb [12].

In this letter, we demonstrate that interband cascade lasers (ICLs) [13,14] relying on interband rather than intersubband transitions can provide both frequency comb operation [15] and a novel NLO platform that does not require external optical pumping. We obtain simultaneous SFG and SHG in an electrically pumped 4 mm long ICL frequency comb, which operates fundamentally around ~3.6 μm with a repetition rate of 9.66 GHz. This device coherently up-converts a 10 milliwatt mid-infrared comb to a second-harmonic near-infrared comb centered around ~1.8 μm, while consuming only 1.5 W of electrical power. The second harmonic comb spectrum covers more than 37 nm (10 dB

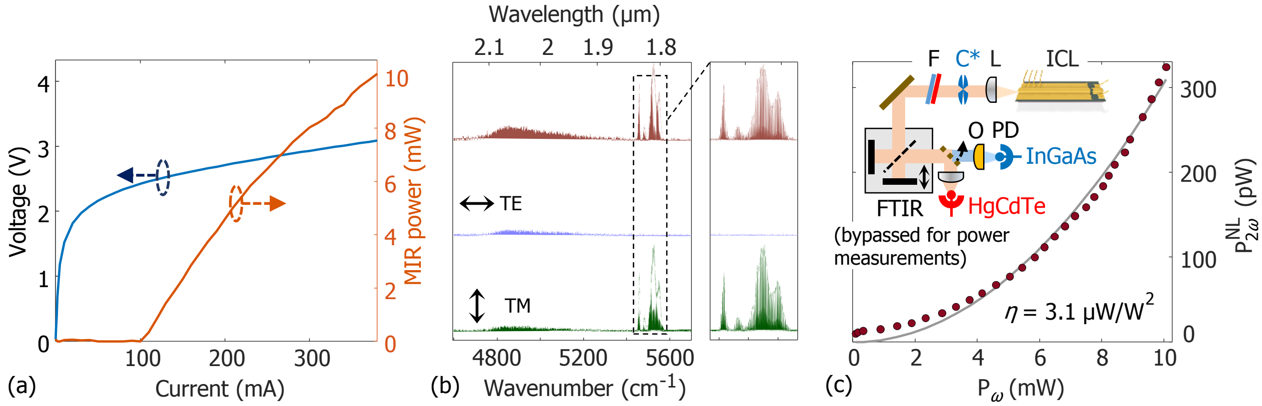

Fig. 1. (a) Power-current-voltage (P-I-V) characterization of the ICL device. (b) Near-infrared part of the optical spectrum at I=380 mA showing the second harmonic spectrum centered at ~1.8 µm characterized by a well-defined polarization together with a broadband incoherent feature around ~2.06 µm attributed to emission from higher electron subbands in the type-II "W" InAs/GaInSb/InAs structure that functions as the active region. The second harmonic light was consequently short-pass-filtered above 1.9 µm in all further experiments. (c) Near-infrared (nonlinear) optical power as a function of mid-infrared (linear) power collected from the front facet along with a least squares parabolic fit. Inset shows the experimental setup.

bandwidth) with two 4-nm wide low-intensity regions, and reaches ~14 nm of 3 dB bandwidth around 1807 nm. Although the generated near-IR power is in the sub-nanowatt regime, significant improvements will be possible via optimization of the phase matching and increasing the intracavity optical power [11]. We validate the potential of this dual-band (octave-spaced) frequency comb by measuring the spectrum of water vapor, which strongly absorbs in the near-IR but not in the mid-IR. The simultaneous dual-band coverage will be highly attractive in future space missions searching for water and organic molecules. The ICL technology has already proven its value on the Mars Curiosity rover mission [16].

Figure 1(a) plots the power-current-voltage (P-I-V) and near-IR spectral characteristics (b) of the ICL grown by molecular beam epitaxy on an n-GaSb substrate, using the design and growth procedures of Ref. [17], which illustrates that 10 mW of cw power is generated. By leaving the short section of the ICL device unbiased, we promote the formation of a frequency-modulated (FM) comb relying on four wave mixing (FWM) [18], while maximizing the optical power for SHG/SFG. We confirmed the comb nature of the source operating in this mode with sub-kilohertz intermode beat note linewidths in a multi-heterodyne (dual-comb) experiment elsewhere [19]. To efficiently collect near-IR light from the ICL output facet, we used a high numerical aperture (NA=0.85) Black Diamond-2 lens (L) with an antireflective coating optimized for 1.8 µm (C037TME-D, Thorlabs). For spectroscopic characterization, whose experimental setup is shown in inset of Fig. 1c, the emitted light was guided over ~1.5 m of free space to a Bruker Vertex 80 Fourier transform spectrometer (FTIR), and focused with a ZnSe microscope objective (O) onto an external extended-InGaAs photodetector (PD, Teledyne Judson, G12182-203K) connected to a lock-in transimpedance amplifier (Stanford SRS-830) synchronized with a mechanical chopper (C*).

To confirm that the generated photocurrent was not produced by two-photon absorption (2PA) of the mid-IR input to the InGaAs photodetector, we placed a 5-mm thick BK-7 glass plate in the beam path, which completely blocked mid-IR light (1% transmission at 3.6 µm) while passing >90% in the near-IR. The detected photocurrent dropped by only ~10% when this filter (F) was introduced. On the contrary, when a long-pass (>2.4 µm) filter that ensured mid-IR illumination only was placed in the beam path, no signal could be detected. Chromatic aberration of the lens that collected the light emitted from the laser facet prevented simultaneous collimation of the near- and mid-IR beams. Hence the mid-IR beam strongly diverged and 2PA was effectively eliminated under the focusing conditions that maximized the near-IR photocurrent.

Figure 1b plots the measured near-IR portion of the spectrum, where in addition to coherent second harmonic light with a well-defined polarization (TM-polarized – orthogonal to the intracavity TE-polarized mid-infrared pump), we observed a broadband asymmetric feature attributable to emission from higher electron subbands in the type-II "W" InAs/GaInSb/InAs structure that functions as the active region. Similar spectral features have been previously observed as a result of electroluminescence from single quantum wells of GaSb/$In_xGa_{1-x}Sb$ in Ref. [15]. We effectively eliminated any contribution of the incoherent longer-wavelength portion of the spectrum to the measured near-IR power characteristics by including a short-pass optical filter with cut-on wavelength of ~1.9 µm (SP-1900 nm, Spectrogon).

Whereas the mid-IR output power (measured with a calibrated power meter) in continuous wave mode at 13°C (Fig. 1a) increases almost linearly with current above the lasing threshold, as expected, the near-IR power plotted in Fig. 1c displays a quadratic dependence on the mid-IR power at a given current. The maximum obtainable power per facet in the near-IR reaches 320 pW at the mid-IR intracavity pump power of 10 mW, which corresponds to a nonlinear conversion efficiency η_{max}=3.2 µW/W^2. The global least-squares parabolic fit (plotted as the solid line) provides a mean efficiency of η=3.1 µW/W^2, which is comparable to the first reports on nonlinearities in QCL structures [7], although it is well short of the efficiencies reaching mW/W^2 that have been reported for optimized structures [21–23]. We attribute the relatively low power to a considerable absorption in the active core and not only in the active wells, but also in the electron injector. Currently, the absorption length in the waveguide is estimated to be ~30 µm at λ=1.8 µm, which may be expected to limit the nonlinear conversion efficiency more than the phase mismatch between the fundamental TE pump and higher order TM signal modes. We postulate that the

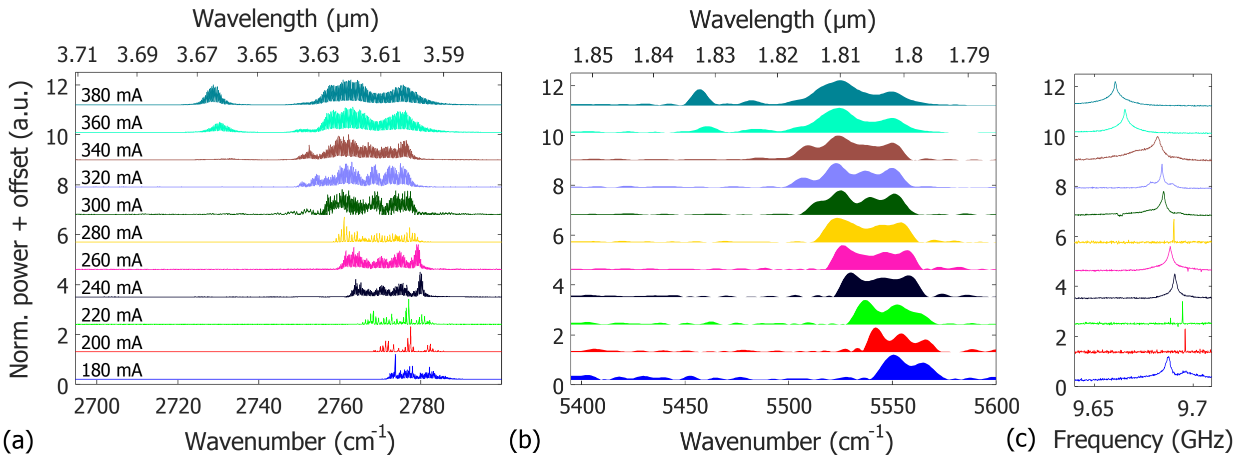

Fig. 2. Evolution of the optical and radio frequency spectrum of a 4 mm long ICL at various currents at 13°C (a) High resolution (0.1 cm^{-1}) spectra in the mid-IR (fundamental frequency); (b) Low resolution (5 cm^{-1}) step-scan spectra in the near-IR (second harmonic); (c). Electrical rf beat note extracted using a bias tee. Several frequency comb regimes with narrow beat note linewidths can be identified.

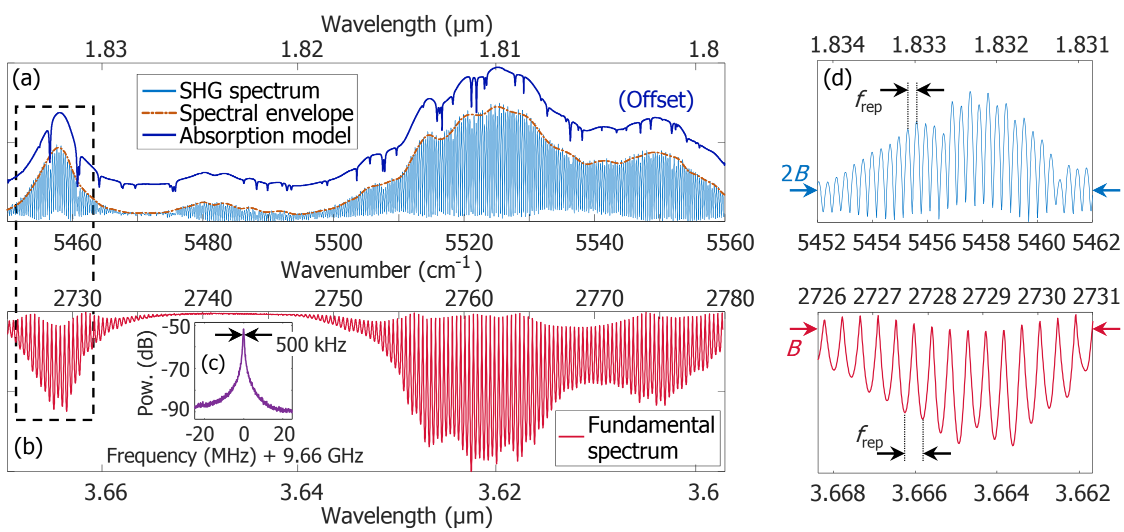

Fig. 3. Simultaneous sum-frequency and second-harmonic generation in the ICL comb biased at I=380 mA (3.5 I_{th}) and 13°C. (a) High-resolution spectrum in the near-IR region; (b) Corresponding mid-IR spectrum; (c) Radio frequency intermode beat notes with ~500 kHz 3 dB linewidth, as measured simultaneously with the optical spectrum; (d) Zoom on the framed parts of both spectra, showing preservation of the mode spacing. The top near-infrared panel has a doubled optical frequency bandwidth (B), and hence possesses twice as many comb lines. Note that some lines are heavily attenuated in the near-IR but not the mid-IR, due to water vapor absorption over the propagation distance to the spectrometer.

intracavity $\chi^{(2)}$ in the ICL is caused by bulk nonlinearity of GaSb separate-confinement layers (SCL). It is inferred from the orthogonality of the near-IR comb polarization, and the large overlap of the mid-IR optical mode with the thick GaSb layers compared to the thin active core, albeit this assertion will require further validation.

Figure 2 plots the mid-IR (a) and near-IR (b) spectral properties acquired with the FTIR for the dual-band ICL comb, together with a microwave intermode beat note spectrum (c) recorded with an electrical spectrum analyzer. Due to the insensitivity of our InGaAs photodetector to mid-IR light, we periodically switched throughout the experiment between a thermoelectrically-cooled HgCdTe detector for rapid high-resolution (0.1 cm^{-1}) mid-IR acquisitions and a step-scan low-resolution (5 cm^{-1}) InGaAs detector for the near-IR. We see from the figure that the near-IR spectrum (Fig. 2b) faithfully follows the shape of the mid-infrared counterpart (Fig. 2a), albeit with a few notable differences. At currents above 360 mA, an additional lobe appears in the mid-IR spectrum that is separated from the dominant bimodal group by more than 30 nm. While this lobe is replicated in the near-IR spectrum, in that case the gap also comes to be populated by optical modes. Not only does this improve the spectral coverage, it also reveals simultaneous SHG and SFG process [24] – a signature of high $\chi^{(2)}$. As the injection current increases, several narrow intermode beat note regimes with near-kHz linewidths are observed (Fig. 2c). This indicates excellent comb coherence properties for dual-comb spectroscopy [19].

The simultaneous occurrence of sum-frequency and second-harmonic generation was investigated further by acquiring high-resolution (0.1 cm^{-1}) spectra for both wavelengths at a current of 380 mA, as shown in Fig. 3. The mirrored spectra for the near-IR (a) and mid-IR (b) are clearly quite similar. However, the additional near-IR feature between about 5472 cm^{-1} and 5492 cm^{-1} must result from SFG between the lower-frequency (on the left) spectral lobe centered on ~2730 cm^{-1} and the lower-frequency portion of the dominant bimodal spectral group beginning at ~2750 cm^{-1}. This conclusion is also supported by the preservation of the mode spacing apparent in panel (d), which would not have been possible had second harmonic generation been solely responsible for generation of the near-IR light. We expect the SFG to be degenerate, since each line in the spectrum can be created by summing different combinations of pump wavelengths [24]. Because SFG and SHG are both coherent second-order nonlinear processes, the near-IR comb should inherit the comb properties of the mid-IR. While the selected comb regime with linewidth ≈ 500 kHz serves as an illustrative example of pronounced SFG, our comb device shows several low-phase noise regimes in which the rf lines are narrower by almost 3 orders of magnitude [15,19].

To demonstrate the spectroscopic potential of our dual-band source, and also to prove unequivocally that the observed near-IR signal is not an artifact arising from photodetector nonlinearities, we measured the absorption by atmospheric water vapor [(011-000) band of $H_2{}^{16}O$)] over a propagation distance of 1.5 m in the proximity of a heated Petri dish filled with water. Using the HITRAN database [25] to model the propagation environment with 45% relative humidity, we simulated the modulation of the envelope spectrum by the absorption profile, as shown by the curve in Fig. 3a. Missing lines in the near-IR spectrum clearly correspond to water vapor features, while the mid-infrared spectrum remains intact and smooth despite propagation in the same environment.

In conclusion, we have demonstrated near-infrared frequency comb generation due to SHG and SFG in a mid-infrared interband cascade laser. The nonlinear conversion efficiency of η=3.2 $\mu W/W^2$ yields 320 pW of near-IR light when the mid-IR output power is 10 mW. We expect that this efficiency can be improved substantially by phase matching the near-IR and mid-IR modes, and by applying highly reflective (HR) coatings to the facets. The near-IR comb centered around 1807 nm has ~14 nm of 3 dB bandwidth and ~37 nm of 10 dB bandwidth with two 4-nm low-intensity wide regions. A detailed evaluation of the near-IR comb properties will be more straightforward once the generated power is higher.

Although the demonstration reported here is preliminary, it paves the way for compact, multi-color ICL frequency comb sources for spectroscopy. The large second order susceptibility $\chi^{(2)}$ may also potentially be used for difference frequency generation, for example, to realize energy-efficient ICL-based THz frequency combs operating with drive powers ≤ 1 W at room temperature.

Funding. National Aeronautics and Space Agency's (NASA) PICASSO program (106822 / 811073.02.24.01.85); Office of Naval Research (ONR); Universities Space Research Association (USRA), NASA Postdoctoral Program (NPP).

Acknowledgment. This work was supported under and was in part performed at the Jet Propulsion Laboratory (JPL), California Institute of Technology, under contract with the NASA. L. A. Sterczewski's research was supported by an appointment to the NASA Postdoctoral Program at JPL, administered by Universities Space Research Association under contract with NASA.

References

1. P. A. Franken, A. E. Hill, C. W. Peters, and G. Weinreich, Phys. Rev. Lett. **7**, 118–119 (1961).
2. T. H. Maiman, Nature **187**, 493 (1960).
3. M. Hentschel, R. Kienberger, C. Spielmann, G. A. Reider, N. Milosevic, T. Brabec, P. Corkum, U. Heinzmann, M. Drescher, and F. Krausz, Nature **414**, 509 (2001).
4. Y. R. Shen, Nature **337**, 519–525 (1989).
5. Y. Okawachi, M. Yu, J. Cardenas, X. Ji, A. Klenner, M. Lipson, and A. L. Gaeta, Opt. Lett. **43**, 4627 (2018).
6. E. Rosencher, A. Fiore, B. Vinter, V. Berger, Ph. Bois, and J. Nagle, Science **271**, 168–173 (1996).
7. N. Owschimikow, C. Gmachl, A. Belyanin, V. Kocharovsky, D. L. Sivco, R. Colombelli, F. Capasso, and A. Y. Cho, Phys. Rev. Lett. **90**, 043902 (2003).
8. M. A. Belkin, F. Capasso, A. Belyanin, D. L. Sivco, A. Y. Cho, D. C. Oakley, C. J. Vineis, and G. W. Turner, Nat. Photonics **1**, 288 (2007).
9. S. Banerjee, P. S. Spencer, and K. A. Shore, Appl. Phys. Lett. **89**, 051113 (2006).
10. K. Fujita, S. Jung, Y. Jiang, J. H. Kim, A. Nakanishi, A. Ito, M. Hitaka, T. Edamura, and M. A. Belkin, Nanophotonics **7**, 1795–1817 (2018).
11. C. Gmachl, A. Belyanin, D. L. Sivco, M. L. Peabody, N. Owschimikow, A. M. Sergent, F. Capasso, and A. Y. Cho, IEEE J. Quantum Electron. **39**, 1345–1355 (2003).
12. Q. Lu, F. Wang, D. Wu, S. Slivken, and M. Razeghi, Nat. Commun. **10**, 2403 (2019).
13. J. R. Meyer, I. Vurgaftman, R. Q. Yang, and L. R. Ram-Mohan, Electron. Lett. **32**, 45–46 (1996).
14. I. Vurgaftman, R. Weih, M. Kamp, J. R. Meyer, C. L. Canedy, C. S. Kim, M. Kim, W. W. Bewley, C. D. Merritt, J. Abell, and S. Höfling, J. Phys. Appl. Phys. **48**, 123001 (2015).
15. M. Bagheri, C. Frez, L. A. Sterczewski, I. Gruidin, M. Fradet, I. Vurgaftman, C. L. Canedy, W. W. Bewley, C. D. Merritt, C. S. Kim, M. Kim, and J. R. Meyer, Sci. Rep. **8**, 3322 (2018).
16. C. R. Webster, P. R. Mahaffy, S. K. Atreya, G. J. Flesch, M. A. Mischna, P.-Y. Meslin, K. A. Farley, P. G. Conrad, L. E. Christensen, A. A. Pavlov, and others, Science **347**, 415–417 (2015).
17. C. L. Canedy, J. Abell, C. D. Merritt, W. W. Bewley, C. S. Kim, M. Kim, I. Vurgaftman, and J. R. Meyer, Opt. Express **22**, 7702–7710 (2014).
18. B. Schwarz, J. Hillbrand, M. Beiser, A. M. Andrews, G. Strasser, H. Detz, A. Schade, R. Weih, and S. Höfling, Optica **6**, 890–895 (2019).
19. L. A. Sterczewski, J. Westberg, M. Bagheri, C. Frez, I. Vurgaftman, C. L. Canedy, W. W. Bewley, C. D. Merritt, C. S. Kim, M. Kim, J. R. Meyer, and G. Wysocki, Opt. Lett. **44**, 2113–2116 (2019).
20. A. Krier, S. A. Bissitt, N. J. Mason, R. J. Nicholas, A. Salesse, and P. J. Walker, Semicond. Sci. Technol. **9**, 87–90 (1994).
21. O. Malis, A. Belyanin, D. L. Sivco, J. Chen, A. M. Sergent, C. Gmachl, and A. Y. Cho, Electron. Lett. **40**, 1586 (2004).
22. O. Malis, A. Belyanin, C. Gmachl, D. L. Sivco, M. L. Peabody, A. M. Sergent, and A. Y. Cho, Appl. Phys. Lett. **84**, 2721–2723 (2004).
23. J. Bai and D. S. Citrin, J. Appl. Phys. **106**, 031101 (2009).
24. J.-Y. Bengloan, A. De Rossi, V. Ortiz, X. Marcadet, M. Calligaro, I. Maurin, and C. Sirtori, Appl. Phys. Lett. **84**, 2019–2021 (2004).
25. L. S. Rothman, I. E. Gordon, Y. Babikov, A. Barbe, D. Chris Benner, P. F. Bernath, M. Birk, L. Bizzocchi, V. Boudon, L. R. Brown, and others, J. Quant. Spectrosc. Radiat. Transf. **130**, 4–50 (2013).